General Disclaimer

One or more of the Following Statements may affect this Document

- This document has been reproduced from the best copy furnished by the organizational source. It is being released in the interest of making available as much information as possible.

- This document may contain data, which exceeds the sheet parameters. It was furnished in this condition by the organizational source and is the best copy available.

- This document may contain tone-on-tone or color graphs, charts and/or pictures, which have been reproduced in black and white.

- This document is paginated as submitted by the original source.

- Portions of this document are not fully legible due to the historical nature of some of the material. However, it is the best reproduction available from the original submission.

Produced by the NASA Center for Aerospace Information (CASI)

NASA TECHNICAL MEMORANDUM

NASA TM X-73606

NASA TM X-73606

(NASA-TM-X-73606) CHARGING CHARACTERISTICS OF MATERIALS: COMPARISON OF EXPERIMENTAL RESULTS WITH SIMPLE ANALYTICAL MODELS (NASA) 29 p HC A03/MF A01 CSCL 22B

N77-19160

Unclas

G3/18 21612

CHARGING CHARACTERISTICS OF MATERIALS: COMPARISON OF EXPERIMENTAL RESULTS WITH SIMPLE ANALYTICAL MODELS

by Carolyn K. Purvis, N. John Stevens,
and Jon C. Oglebay
Lewis Research Center
Cleveland, Ohio 44135

MAR 1977
RECEIVED
NASA STI FACILITY
INPUT BRANCH

TECHNICAL PAPER presented at the
Spacecraft Charging Technology Conference cosponsored by the
United States Air Force and National Aeronautics and Space Administration
Colorado Springs, Colorado, October 27-29, 1976

E-8970-2

CHARGING CHARACTERISTICS OF MATERIALS: COMPARISON OF EXPERIMENTAL RESULTS WITH SIMPLE ANALYTICAL MODELS

by Carolyn K. Purvis, N. John Stevens, and Jon C. Oglebay

National Aeronautics and Space Administration
Lewis Research Center
Cleveland, Ohio 44135

ABSTRACT

An understanding of the behavior of materials, of dielectrics in particular, under charged particle bombardment is essential to the prediction and prevention of the adverse effects of spacecraft charging. This paper presents an effort to obtain such an understanding through a combined analytical and experimental approach. A one-dimensional model for charging of samples in the LeRC test facility is used in conjunction with experimental data taken in this facility to develop "material charging characteristics" for silvered Teflon. These characteristics are then used in a one-dimensional model for charging in space to examine expected response. Relative charging rates as well as relative charging levels for silvered Teflon and metal are discussed.

1. INTRODUCTION

Two previous papers[1,2] described the test facility, test methods and measurements, and the results of various materials characteristics tests performed at the Lewis Research Center in support of the spacecraft charging investigation. The present paper summarizes the analytical work which has been performed interactively with this experimental work. The goal of the analysis is twofold. First, is to model the charging of material samples in terms of the material's parameters. Second, since a goal of the entire study is to predict behavior of spacecraft surfaces, an attempt is made to "scale" the environment, that is, to relate results obtained using a monoenergetic beam in the ground test facility to expected results with distributed particle fluxes of the space environment. An approach to establish this environment scaling is to develop models of charging for both charged particle environments, and assume that the material properties are constant. Then differences between material charging behavior underground test and in space are a result of the differences in the two environments. It is recognized that the vacuum levels in the ground test and space environments are also different. No attempt is made here to account for this factor.

*Published in the proceedings of the Conference on Spacecraft Charging Technology, NASA TM X-73537, 1977.

STAR Category 18

This paper, then, represents a first attempt at attaining the two goals of characterizing material charging and scaling to the space environment. The models used are one-dimensional, and describe charging of samples in terms of the charging of a capacitor. This type of model has been used by a number of workers[3,4,5,6] to describe spacecraft charging.

The procedure used herein was to first develop a one-dimensional model to describe charging of samples in the LeRC vacuum test facility. This model contained a number of parameters which were varied to provide best fits to experimental data obtained in the facility. The values of these parameters which yielded the best fit were identified as the "material charging characteristics." These were then used in conjunction with a one-dimensional model for charging in the space substorm environment to make some predictions of the charging behavior of the materials in space. The insulator studied here is 5 mil silvered FEP Teflon®

2. ONE-DIMENSIONAL (1-D) GROUND TEST FACILITY MODEL

In the LeRC test facility, a monoenergetic beam of electrons with energies of ~2 to 20 keV is directed at normal incidence to planar samples. A beam current density of 1 nA/cm^2 was used to obtain all test data discussed in this report.

The Ground Test Facility Model is a quasistatic current balance model. The current densities considered are those due to primary (beam) electrons, secondary electrons, backscattered electrons, and leakage current through the sample bulk. These are denoted by j_e, j_s, j_{BS}, j_ℓ, respectively. The sample is assumed to charge like a capacitor. Thus, a time balance equation is of the form

$$C \frac{dV_S}{dt} + j_\ell = j_e - j_s - j_{BS} \tag{1}$$

where V_S is the magnitude of the surface voltage. All signs are explicit in this equation, and in all others used in the test facility model, that is, all symbols stand for positive numbers. The actual surface voltage is of course negative, and this is assumed throughout. Thus, this model does not predict positive surface voltages correctly, since positive surface voltage would tend to reattract the emitted secondary electrons and this effect has not been included here.

The first term in equation (1) represents the net charge deposited on the surface (per cm^2) in a time step, and so is termed the charging

current density, and denoted by j_c. The procedure used was to initialize at $t = 0$ with $V_S = 0$. Then ΔV_S was calculated from

$$\frac{\Delta V_S}{\Delta t} = \frac{1}{C}\left[j_e - j_s - j_{BS} - j_\ell\right] \tag{2}$$

The current densities are all functions of V_S. Their functional forms are given in figure 1. Equation (2) is solved by an iterative procedure. This equation can be expressed as

$$\Delta V_S = f(V_S)\Delta t \tag{2a}$$

With the initial assumption $V_S = t = 0$, a suitable Δt is chosen, and ΔV_S calculated. V_S is then incremented by ΔV_S (set = ΔV_S for the first iteration) and the procedure repeated until equilibrium is reached, that is, until $j_c \geq C\, dV_S/dt = 0$.

The several current densities in the above equations are functions of surface voltage. All but the leakage current density are functions of the primary electron beam voltage and current density. The parameters which can be varied are the secondary emission maximum yield, δ_m, and energy for maximum yield, V_m, the backscatter coefficient, ζ, the resistivity, ρ, and the capacitance C. In practice, values for δ_m and V_m were taken from the literature; values for ρ were determined from the measured surface voltages and currents at equilibrium, and fits obtained by varying ζ and C. This is discussed more fully in section 4 below.

It should be noted that this model does not account for beam spread in angle or energy, the presence of the vacuum tank walls, or residual gas in the chamber. Since it is one-dimensional, it cannot, of course, explicitly describe edge effects, or effects due to surface variations.

Derivations of the current density equations are presented in Appendix A; a summary of the model and equations is given in figure 1.

3. COMPARISON WITH EXPERIMENTAL DATA

3.1 "Floating" Aluminum Plate

The first test data used in conjunction with the test facility charging model were those taken with a bare aluminum plate which is normally used for substrates. This plate was mounted in front of a second identical plate which was grounded to the chamber walls. These two

plates were held apart and electrically isolated by a Teflon spacer plug 0.7 cm long. The plates are rectangular, with dimensions 15 cm x 20 cm (~300 cm^2 area). Surface voltage of the floating plate was measured as a function of time using the surface voltage probe[1].

Figure 2 shows these data and the best fit calculated curves. In obtaining these fits to the data values of $\delta_m = 3$ and $V_m = 400$ were used. These are consistent with ranges of values for these parameters given by Gibbons[7] for a surface layer of Al_2O_3. It is reasonable to expect some oxide on the surface of the "bare aluminum" plate since it had in fact been exposed to air. This points up the strong dependence of charging phenomena on sample surface condition, and indicates that care must be taken in making predictions for charging to consider the state of the surface.

With these values in the expression for secondary emission, the values of C used to obtain the curves in figure 2 varied from 1.2×10^{-10} farads at $V_B = 5$kV to 5×10^{-11} farads at $V_B = 16$ kV, decreasing approximately linearly with increasing beam voltage. The values used for the "backscatter coefficient" varied from 0.15 at $V_B = 5$kV to 0.5 at $V_B = 16$ kV, again in approximately linear fashion. The expression used to calculate secondary emission current density is derived from an expression for yield as a function of primary energy due to Sternglass[8]. It is plausible that the required variation of ζ to obtain fits to the data is accounted for, in part, by deviations of the actual secondary yield from that predicted by Sternglass formula. That is, the adjustments to ζ represent adjustments to the sum of the backscattered and secondary electrons.

The final point of concern here is the time scale for charging of the floating plate; it reaches its equilibrium floating voltage with a time constant of several seconds. This is not surprising, since the capacitance of the test plate to its surroundings is expected to be small. The time scale is relevant, however, to the question of the behavior of composite samples. This is discussed more fully in section 3.3 below.

3.2 Silvered Teflon Samples

The 1-D model was next used to fit current and surface voltage data from silvered Teflon samples. These consist of an aluminum substrate with three strips of 5 mil silvered Teflon mounted with conductive adhesive to the substrate. Each of these strips was 5 cm wide and 20 cm long. During test, the aluminum substrate (and consequently the silver) was grounded, while the Teflon surface was bombarded with electrons.

The data and calculated fits for beam voltages at which equilibrium is reached are shown in figure 3. These data are a composite of four separate data sets, and indicate charging times on the order of minutes. The error bars reflect the scatter in the data as well as the $\pm 5\%$

resolution uncertainty in the voltage measurements. Since for insulators there are strong voltage gradients near the edges of the samples, the surface voltage measurements are those read at the sample center which is uniform.

To obtain these curves, the effective resistance was calculated from the equilibrium values of surface voltage and leakage current. These values indicate an effective resistivity for the samples of about 9×10^{15} Ω-cm, about an order of magnitude below published values for Teflon. If one assumed that the published value of 10^{17} Ω-cm is accurate, then a parallel path having a resistance of about 4×10^{11} Ω is indicated by the data. This could be a surface leakage, or an edge leakage, or leakage through the sheath.

Values of $\delta_m = 3$ and $V_m = 300$ were used in the expression for secondary emission, in accordance with the data given by Willis and Skinner[9]. The values of C required ranged from 14.6 pf/cm^2 at $V_B = 5$ kV to 10 pf/cm at $V_B = 12$ kV and decreased monotonically with increasing beam voltage. Extrapolation of the curve to $V_B = 0$ indicates a dielectric constant for Teflon of ~2.1. This decrease in effective capacitance is believed to be associated with edge effects. Edge gradients are observed in the data. These become more pronounced at higher voltages, reducing the effective area[2]. The value used for the backscatter coefficient varies about an order of magnitude for the Teflon samples. Not only does it change with beam voltage, but also appears to change during charging at a single beam voltage. For the initial portion of the charging curves, ζ varied from 0.25 at the lower beam voltages to 0.05 at high beam voltages. At equilibrium, ζ varied from 0.2 at low beam voltages to 0.25 at high ones. These variations were not linear; rather, ζ was relatively constant at low and high beam voltages, with a transition occurring between $V_B = 8$ kV and $V_B = 12$ kV. Again, part of these variations may be due to deviations of the actual secondary emission from that calculated by the analytical expression being used.

Some investigation was undertaken to study the behavior of the Teflon samples during arcing. Figure 4(a) shows a curve fit to a composite of two data sets for the initial charging transient with a beam voltage of 16 kV. Figure 4(b) shows the same calculated curves, this time with a single set of data. The left hand set of curves and points are the initial charging transient. An arc occurred on this sample between the time of the voltage reading at $t = 4$ min and that of the current reading taken at $t = 5\frac{1}{2}$ min; the surface discharged, and charging was repeated. The curves shown for the post-arc charging transient are identical to those for the initial transient, but shifted in time. This indicates that the charging transient is quite repeatable, not only from test to test of Teflon samples, but also through arcing. That is, at least short term, the arcing does not affect the charging behavior of Teflon samples.

3.3 Composite Sample

One of the stated objectives of the present work was to investigate the "environment scaling" effects between the ground test and space environments. An obvious difference other than the environment between ground tests so far described and the space condition is that the studies of silvered Teflon discussed above were all conducted with the substrate grounded. In contrast, for the case of a spacecraft in orbit, the entire body, including the "grounds" must come into equilibrium with the charged particle environment. The question of the behavior of a composite system becomes particularly interesting because of the divergent time scales in which charging of "floating" metal plates and silvered Teflon above ground are observed to occur.

To investigate this question, a composite sample was built and tested. The sample consisted of an electrically floating standard aluminum substrate with two strips of the 5 cm silvered tape mounted on it. This allowed for a 5 cm strip of the aluminum between the two Teflon strips to be exposed to the electron beam. The aluminum substrate was mounted in the test chamber in the same manner as the floating aluminum plate described in section 3.1. This configuration is depicted at the top of figure 5(a). The bottom of this figure shows a voltage trace at equilibrium for this sample.

The expectation was that this composite sample would charge in two stages because of the different effective capacitances through which the aluminum and the Teflon must charge. The prediction, shown in figure 5(b), is based on the idea that when the beam is turned on, the aluminum should charge to its equilibrium voltage with its time constant of seconds, carrying the Teflon voltage with it. When this has occurred, the Teflon should continue to charge from the equilibrium voltage of the aluminum to its own equilibrium voltage with its own time constant, that is, minutes. The curves in figure 5(b) were thus obtained by superimposing the curves for aluminum alone and for Teflon alone with the Teflon curve shifted, so that it coincides with the aluminum curve at the point of equilibration for the aluminum. As can be seen from the data plotted in this figure, the expected behavior was found.

The expectation that the aluminum and Teflon comprising the composite sample should charge to the same surface voltages as had the floating plate and the Teflon samples above grounded substrates was based on the observation that in both those cases the equilibration was dominated by secondary emission phenomena rather than by leakage currents to ground. This is evidenced in two ways. First, plots of surface voltage at equilibrium versus beam voltage are straight lines; such behavior is supposed to be associated with emission dominated equilibration. Second, examination of printouts of the model calculations reveals that, at equilibrium, the leakage current density term is several orders of magnitude smaller than the other currents in the model. The conclusion, then, is that for this type of composite sample, each part responds to the

charging environment with its characteristic time constant, and comes into equilibrium at its characteristic surface voltage so long as leakage current does not play a dominant role in the equilibration.

It should be noted here that the tests run on this composite sample were not extensive. Further experimental investigation of this and other composite samples are planned.

4. ONE-DIMENSIONAL SPACE CHARGING MODEL

In order to predict charging behavior in space, a one-dimensional model for charging in space analogous to the one-dimensional ground test model was developed. The essential difference between the two models, is that, the space model assumes an isotropic Maxwellian particle distribution containing both electrons and ions, and a spherical collection geometry. The current densities are derived from Langmuir probe calculations. This type of calculation has been used by several authors[4,5,6,10] to treat the spacecraft charging problem. Derivation of the current density equations is given in Appendix B; a summary description is presented as figure 6. As is indicated in this figure, the model as presented and used here assumes a geomagnetic substorm condition. That is, it assumes that V_S is negative, so that electrons are repelled and ions attracted. In these equations V_S is an algebraic quantity, that is, the sign is implicit.

As is evident from the sketch in figure 6, secondary electrons due to ion impact are not accounted for in this model. This is because the intent here is to use material charging characteristics found by fitting the ground test model to experimental data in conjunction with the space model to predict space charging. Since there were no ions used in the experiments, no coefficient for secondary electrons due to ion impact was determined. Therefore, this current density source is not considered. The surface voltage values predicted by this model are therefore somewhat larger than if secondary electrons due to ion impact had been included. For example, a secondary coefficient of 1 would yield about 10% reduction in the equilibrium voltage calculated for aluminum at $V_e = 5$ kV.

The procedure used to calculate charging is identical to that described for the ground test model. Material characteristics used were those determined by fitting the ground test model to the data. The capacitance of the aluminum (considered to represent the spacecraft "ground") was taken to be 15×10^{-11} farads, which is the capacitance of a 1 meter diameter sphere (to represent a "typical" spacecraft dimension) to infinity. This capacitance was chosen because the relevant capacitance for charging floating metal objects is that of the object to its surroundings. Those parameters (notably C and ζ for Teflon, and ζ for aluminum) which varied as functions of beam (and therefore surface) voltage were associated with the equilibrium surface voltage for the

appropriate test for purposes of making the space voltage calculations. The relationships between electron and ion temperatures and between temperatures and current densities were taken from the Provisional Specification for the Geomagnetic Substorm Environment.[11] This Specification is given as figure 7. Thus, results of the space calculations, shown in figure 8, are given as functions of electron temperature only.

In figure 8(b) two curves are shown for the surface voltage of silvered Teflon as a function of electron temperature. The first curve calculated used the experimentally determined value of 9×10^{15} Ω-cm for the effective resistivity of Teflon. This curve bends sharply to the right as electron temperature increases. An inspection of the current densities driving the equilibrium indicated that leakage current played a large part in the equilibration of the Teflon. Thus, this curve yields a "good" value for the surface voltage of Teflon if the spacecraft "ground" is actually near plasma ground. This would be the case if, for example, photoemission were holding the spacecraft ground near plasma ground and the Teflon surface of concern were shaded. However, if the spacecraft is assumed to be in eclipse, the aluminum representing the spacecraft ground is predicted to acquire a large negative voltage (solid line). In this case, it is clear that leakage current cannot drive the equilibration of the Teflon surface according to the dashed line. Therefore, a second curve was calculated for the Teflon, based on the assumption that there was no leakage. This is shown in the dash-dotted line.

Figure 8(a) shows the rates of charging predicted for the space condition. The time to charge the aluminum is predicted to be seconds, comparable to the time required to charge the floating plate in the ground experiments. The time required to charge the Teflon is predicted to be several minutes at lower electron temperatures, ranging to tens of minutes as the electron temperature increases. Thus, equilibration of Teflon is predicted to require significantly longer time in space than it does in ground experiments.

Using the curves shown in figure 8, it is possible to predict the response of a "spacecraft," composed of an aluminum structure partially covered with silvered Teflon, to substorm and eclipse conditions. Such a set of predictions is shown in figure 9. For purposes of this figure it is assumed that photoemission is sufficient to hold illuminated surfaces close to plasma ground.

Figure 9(a) assumes that the Teflon surface of interest is shaded when the spacecraft is in sunlight. A substorm injection with a 5 keV Maxwellian electron distribution is assumed to occur at $t = 0$ and this environment is assumed to remain constant throughout the time shown. An eclipse is assumed to occur from $t = 60$ minutes to $t = 120$ minutes. When the substorm occurs, the dark Teflon charges according to the dashed curve of figure 8(a), shown in figure 9 as a solid curve; the aluminum at "ground" is assumed to be held near plasma ground by

photoemission. The Teflon surface reaches its leakage dominated equilibrium voltage of -8.5 kV with its time constant of about 20 minutes. When the spacecraft enters eclipse, the aluminum charges quickly (in seconds) to its equilibrium voltage of -10 kV. It is assumed that the charge on the Teflon surface is immobile on this time scale, so this surface remains at -8.5 kV. At this point, the leakage current, which was driven by the voltage differential of 8.5 kV disappears, so the Teflon finds itself to be no longer in equilibrium with its environment and proceeds to charge to its "floating" value of ~-14.5 kV in a characteristic 20-30 minute period. Upon exit from eclipse, a similar pattern is followed. The aluminum falls quickly to near plasma ground. Because this discharging is driven by photoemission, it requires only about 0.02 second for the aluminum to reach plasma ground (assuming $\sim 10^{-9}$ amps/cm^2 photocurrent). Now, the Teflon again finds itself out of equilibrium with its plasma environment, and proceeds to discharge slowly to its previous equilibrium potential of -8.5 kV.

Figure 9(b) shows a similar type of time history for an insulating surface which is exposed to sunlight. Again, the solid line represents the surface voltage of the Teflon and the dashed line the spacecraft ground. The entry into eclipse and subsequent charging up is analogous to the charging of the composite sample discussed in section 4 above. The aluminum charges rapidly (in seconds) to its equilibrium value. Because the Teflon had no significant charge on its surface, its voltage follows that of the aluminum until the aluminum reaches equilibrium. The Teflon then continues to charge slowly to its equilibrium potential. Upon exit from eclipse, both the aluminum and the Teflon are discharged by photoemission. Thus, the aluminum reaches a plasma ground in about 0.02 second, as in the previous case. The Teflon also discharges more quickly than it charged; it requires about 4 minutes to reach plasma ground.

These results indicate a need for charging studies which take into account relative charging rates as well as different equilibrium charging levels of various spacecraft surfaces. A "typical" spacecraft has several different types of surfaces (solar cells, thermal blankets, etc.) each of which can be expected to charge with its own time constant. The importance of the effect of the different time constants should be assessed.

5. CONCLUDING REMARKS

The present study has resulted in the development of a set of "material charging characteristics" which describe the charging of small (300 cm^2) samples of 5 mil silvered Teflon and oxidized aluminum. Based on these characteristics, predictions of charging in space have been made and used to estimate the behavior of a composite body under conditions of substorm and eclipse. Several interesting differences between charging

behavior under ground test conditions and predicted behavior in space have been noted for silvered Teflon. Under ground test conditions silvered Teflon acquires the same surface potential mounted on grounded and floating substrates because the equilibration is dominated by surface emission phenomena. However, in space, significant differences are predicted in surface voltage for these two mounting configurations. This is because leakage current dominates the equilibration of the Teflon when the aluminum is at ground, while surface emission dominates for the floating aluminum case. The time required for silvered Teflon to charge to equilibrium in tests is several minutes; this time is predicted to be several tens of minutes in space.

In contrast to the several minutes to several tens of minutes time scales for silvered Teflon, floating aluminum samples are observed in ground test and predicted in space to charge to equilibrium in seconds. Their capacitance is much lower than that of Teflon since it is determined by their surroundings. There are also orders of magnitude differences in time scales for discharging by photoemission of aluminum and Teflon. This discrepancy in charging and discharging rates gives rise to sudden changes in the electric fields which the Teflon must sustain upon entry into and exit from eclipse. It is felt that these differential charging rates as well as differential charging levels may be important and should be investigated further. Thus, transient (quasi-static) as well as steady state models should be developed for charging.

The one-dimensional models described herein have been found useful in the interpretation of experimental results, and as guides to relating test results to expected space behavior. Models of ground test situations are needed since they can be used interactively with test data. This is especially true since it is impossible, or at least impractical, to simulate accurately the geosynchronous environment. Thus, environment scaling must be done through use of models, at least for the present.

Finally, higher dimensional models are needed. One-dimensional models cannot account for such things as edge effects or interactions between adjacent surfaces at different potentials as with different charging properties. Such effects are clearly important,[2] and may dominate the charging behavior of multi-surface samples and spacecraft.

REFERENCES

1. Berkopec, F. D., Stevens, N. J., and Sturman, J. C. (1976) The LeRC Substorm Simulation Facility, Paper III-1 presented at the Spacecraft Charging Technology Conference, Colorado Springs, Colorado.

2. Stevens, N. J. et al. (1976) Testing of Typical Spacecraft Materials in a Simulated Substorm Environment, Paper 111-2 presented at the Spacecraft Charging Technology Conference, Colorado Springs, Colorado.

3. DeForest, S. E. (1972) Spacecraft Charging at Synchronous Orbit, J. Geophys. Res. 77: 651-659.

4. Fredericks, R. W. and Scarf, F. L.: (1973) Observations of Spacecraft Charging Effects in Energetic Plasma Regions, in Photon and Particle Interactions with Surfaces in Space, R. J. L. Grard, Ed., D. Reidel Pub. Co., Dordrecht, Holland.

5. Inouye, G. T. (1975) Spacecraft Charging Model. AIAA Paper 75-255, AIAA 13th Aerospace Sciences Meeting, Pasadena, California.

6. Inouye, G. T. (1975) Spacecraft Charging: Environment Induced Anomalies, AIAA Paper 75-91, AIAA 13th Aerospace Sciences Meeting, Pasadena, California.

7. Gibbons, D. J.: (1966) Secondary Electron Emission, in Handbook of Vacuum Physics, Vol 2, A. H. Beck, Ed., Pergamon Press, Oxford, England.

8. Sternglass, E. J.: (1950) Secondary Electron Emission and Atomic Shell Structure, Phys. Rev. 80: 925-926.

9. Willis, R. F. and Skinner, D. K.: (1973) Secondary Electron Emission Yield Behavior of Polymers, Solid State Communications 13: 685-688.

10. Cauffman, D. P.: (1975) Inclusion of Secondary Electrons in Models of Equilibrium Potentials. Paper SA63 presented at the spring AGU meeting Washington, D. C.

11. Lovell, R. R., Stevens, N. J. and Purvis, C. K. (1976) Provisional Specification for Satellite Time in a Geomagnetic Substorm Environment, Paper V-2 presented at the Spacecraft Charging Technology Conference, Colorado Springs, Colorado.

12. Mott-Smith, H. M. and Langmuir, I.: (1926) The Theory of Collectors in Gaseous Discharges, Phys. Rev. 28 727-763.

13. Grard, R. J. L., Knott, K., and Pederson, A.: (1973) The Influence of Photoelectron and Secondary Electron Emission on Electric Field Measurements in the Magnetosphere and Solar Wind, in Photon and Particle Interaction with Surfaces in Space, R. J. L. Grard, Ed., D. Reidel, Dordrecht, Holland.

14. Abramowitcz, M. and Stegun, I. A., eds.: (1968) Handbook of Mathematical Functions, Dover Publications, Inc., New York.

APPENDIX A

ONE-DIMENSIONAL GROUND TEST MODEL

A.1. INTRODUCTION

In this model, electrons from the electron gun are assumed to approach the planar sample normally. All motion is restricted to the x direction (see fig. A.1). The electron beam is assumed momoenergetic, with energy

$$\varepsilon_B \triangleq eV_B$$

where e is the electronic charge and V_B the beam voltage. The current density emitted from the gun is given by

$$j_o = N_o e \left(\frac{2\varepsilon_B}{M_e}\right)^{1/2} \tag{A1}$$

where N_o = particle density. It is assumed here that $N_o e$ (the charge density) is constant. Thus, the continuity equation requires that some particles are "lost."

We wish to calculate current densities to the sample surface. Current densities to be considered are those due to primary electrons, secondary electrons, backscattered electrons and leakage through the bulk of the insulator. The insulator is assumed to be mounted above a grounded substrate for purposes of calculating leakage.

Throughout this development the sample surface is assumed negative, and all secondary and backscattered electrons are assumed to escape. All signs are given explicitly, so that, symbols represent positive quantities.

A.2 CURRENT DENSITY DUE TO PRIMARY ELECTRONS

Consider electrons approaching the sample with energy ε. It is assumed that the electrons do not collide with one another, and that motion is restricted to one dimension. If the sample surface has a repulsive potential of magnitude V_S, energy conservation requires that they arrive at the surface with energy $\varepsilon - eV_S$. Since all electrons leave the gun with energy eV_B, the current density to the sample surface is simply

$$j_e = N_o e \left(\frac{2}{M_e}\right)^{1/2} (eV_B - eV_S)^{1/2} \tag{A2}$$

Rearranging and using equation (A1), we find

$$j_e = j_o \left(1 - \frac{V_S}{V_B}\right)^{1/2} \tag{A3}$$

A.3 CURRENT DENSITY DUE TO SECONDARY ELECTRONS

Sternglass[8] has given the following expression for secondary yield as a function of primary electron energy at impact:

$$\delta(\varepsilon_i) = 7.4\ \delta_m \frac{\varepsilon_i}{eV_m} \exp\left[-2\left(\frac{\varepsilon_i}{eV_m}\right)^{1/2}\right] \tag{A4}$$

where δ_m is the maximum yield, eV_m is the primary energy for which maximum yield is attained and ε_i is primary energy at impact. From the discussion given in (A2) above, for this case

$$\varepsilon_i = eV_B - eV_S \tag{A5}$$

The secondary current density is then

$$j_s = j_e\ \delta(eV_B - eV_S) \tag{A6}$$

which is

$$j_s = j_o\ 7.4\ \delta_m \frac{V_B}{V_m}\left(1 - \frac{V_S}{V_B}\right)^{3/2} \exp\left[-2\left(\frac{V_B - V_S}{V_m}\right)^{1/2}\right] \tag{A7}$$

A.4 CURRENT DENSITY DUE TO BACKSCATTERED ELECTRONS

No analytical expression was found for backscattered electron emission. For simplicity, it was therefore assumed that backscattered electron current density represents a fraction of the incident current density. Thus,

$$j_{BS} = \zeta j_e = \zeta j_o \left(1 - \frac{V_S}{V_B}\right)^{1/2} \tag{A8}$$

A.5 LEAKAGE CURRENT DENSITY

Leakage current is generally represented by

$$i_\ell = \frac{V_S}{R} \tag{A9}$$

In terms of bulk resistivity this is

$$i_\ell = \frac{V_S A}{\rho \ell} \tag{A10}$$

where ρ is bulk resistivity, A is the area and ℓ the thickness of the sample. Then

$$j_\ell = \frac{i_\ell}{A} = \frac{V_S}{\rho \ell} \tag{A11}$$

A.6 THE 1-D MODEL

The primary electron current density represents a source of electrons arriving at the sample. The other three current densities represent loss of electrons from the surface. Thus, the net current density to the surface is

$$j_C = j_e - j_s - j_{BS} - j_\ell \tag{A12}$$

This net current density plays the role of a charging current to the surface. Thus, if we represent the sample's charging as the charging of a capacitor, we have

$$j_C = C \frac{dV_S}{dt} = j_e - j_s - j_{BS} - j_\ell \tag{A13}$$

where C is capacitance, here expressed in farads per square centimeter to maintain consistency of units. Equation (A13) is solved in the manner described in the text on a computer to calculate the charging.

It remains to associate the experimentally measured parameters, surface voltage, and total current to ground, with calculated values. The surface voltage association is trivial; it is simply $-V_S$. The

total current to ground is the charging current plus the leakage current for the sample as a whole. Thus,

$$I_m = A(j_c + j_\ell) \tag{A14}$$

APPENDIX B

ONE-DIMENSIONAL SPACE SUBSTORM MODEL

B.1 INTRODUCTION

The one-dimensional space model assumes a two-dimensional isotropic Maxwellian velocity distribution for primary particles, and a spherical collection geometry. The calculations are essentially those for a spherical Langmuir probe. The present calculations are based on the work of Langmuir[12] and Grard, et al.[13] and follow closely the derivation of Cauffman.[10] The latter work has not been published; therefore, portions of it are reproduced here for clarity. Such portions are identified by superscript reference.

Geometry for the calculations is depicted in figure B.1.[10] The sheath is assumed to have radius a, the collector radius R. The radial and tangential velocity components in the "undisturbed" region (sheath edge) are v_r and v_t, respectively and those at the collector surface u_r and u_t. The surface potential of the collector is V_S. The potential in the sheath is assumed to be a function of radial distance from the collector and to be monotonic. The plasma is assumed collisionless, that is, orbit limited theory applies, and energy and angular momentum are assumed constant for each particle.

The integral requiring solution for current densities due to primary electrons[10,13] and ions, and backscattered electrons is

$$j_i = \frac{i_i}{4\pi R^2} = \frac{4\pi a^2}{4\pi R^2}\int_0^{\pi/2} d\theta_R \int_0^{\infty} d\varepsilon_R \frac{dj_i}{d\varepsilon_R}(\varepsilon_R,\theta_R) \tag{B1}$$

where the subscript i stands for either e (electrons) or p (H^+ ions), and θ_R and ε_R are the angle and energy at impact on the collector (see fig. B1).

For secondary electron current, solution must be found for [10,13].

$$j_s = \frac{i_e}{4\pi R^2} = \frac{4\pi a^2}{4\pi R^2}\int_0^{\pi/2} d\theta_R \int_0^{\infty} d\varepsilon_R \frac{dj_e}{d\varepsilon_R}(\varepsilon_R,\theta_R)\delta(\varepsilon_R) \tag{B2}$$

where $\delta(\varepsilon_R)$ is the secondary electron yield as a function of electron impact energy.

These integrations cannot be performed directly because the distribution function for the particles at the collector is unknown, and therefore we can not determine $dj_i/d\varepsilon_R$. However, we do know the distribution at the sheath edge, and can therefore determine $dj_i/d\varepsilon_a$. If we assume the plasma to be collisionless, we can also convert the limits on ε_R and θ_R to limits on ε_a and θ_a, and perform the required integrations on these variables.

B.1.1 Conditions for Collection

In order to contribute to current collected at R, a particle must have energy $\varepsilon_R \geq 0$ and direction $0 \leq \theta_R < \pi/2$. Since the plasma is assumed collisionless and $V(r)$ is assumed monotonic, each particle's energy and angular momentum must be conserved. Assume the particles of interest have charge $-e$. Energy conservation demands

$$\frac{1}{2} M_i(u_r^2 + u_t^2) = \frac{1}{2} M_i(v_r^2 + v_t^2) + eV_S \Leftrightarrow \varepsilon_R = \varepsilon_a + eV_S \tag{B3}$$

Angular momentum conservation demands

$$Ru_t = av_t \Leftrightarrow Ru \sin\theta_R = av \sin\theta_a \tag{B4}$$

where

$$u = (u_r^2 + u_t^2)^{1/2} \quad \text{and} \quad v = (v_r^2 + v_t^2)^{1/2}$$

Solving for ε_a and θ_a in terms of ε_R and θ_R yields the conditions for collection[10]

$$0 \leq \theta_R \leq \frac{\pi}{2} \Rightarrow 0 \leq \theta_a \leq \sin^{-1}\left[\frac{R}{a}\left(\frac{\varepsilon_a + eV_S}{\varepsilon_a}\right)^{1/2}\right] \triangleq \theta_o$$

$$\infty > \varepsilon_R \geq 0 \Rightarrow \infty > \varepsilon_a \geq \varepsilon_o \triangleq \begin{cases} 0 & \text{for } V_S \geq 0 \text{ (attraction)} \\ -eV_S & \text{for } V_S \leq 0 \text{ (repulsion)} \end{cases} \tag{B5}$$

B.1.2. Energy Format

An isotropic Maxwellian velocity distribution in three dimensions has a distribution given by

$$f(\vec{v}) = \left(\frac{M_i}{2\pi eV_i}\right)^{3/2} \exp\left[-\frac{M_i\vec{v}\cdot\vec{v}}{2eV_i}\right] \tag{B6}$$

We are interested in a two-dimensional distribution which can be found from

$$g(v_r,v_t) = \int_0^{2\pi} f(v_r,v_t \sin\psi, v_t\cos\psi)d\psi \tag{B7}$$

Substituting for $f(\vec{v})$ and integrating, we have

$$g(v_r,v_t) = \frac{1}{\sqrt{2\pi}}\left(\frac{M_i}{eV_i}\right)^{3/2} v_t \exp\left[-\frac{M_i(v_r^2+v_t^2)}{2eV_i}\right] \tag{B8}$$

Langmuir[12] gives the incremental current across the sheath as

$$di = 4\pi a^2 Nev_r g(v_r,v_t)dv_r dv_t \tag{B9}$$

Then,

$$dj_i = \frac{di_i}{4\pi R^2} = \frac{a^2}{R^2}\frac{N_i e}{\sqrt{2\pi}}\left(\frac{M_i}{eV_i}\right)^{3/2} v_r v_t \exp\left[-\frac{M_i(v_r^2+v_t^2)}{2eV_i}\right] dv_r dv_t \tag{B10}$$

and, changing to ε_a, θ_a coordinates we have[10]

$$dj_i = \frac{a^2}{R^2} N_i e \left(\frac{eV_i}{2\pi M_i}\right)^{1/2} \frac{2}{(eV_i)^2}\,\varepsilon_a \exp\left[-\frac{\varepsilon_a}{eV_i}\right] \sin\theta_a\cos\theta_a d\theta_a d\varepsilon_a \tag{B11}$$

as required.

B.2 PRIMARY AND BACKSCATTERED PARTICLE CURRENT DENSITIES

Since backscattered electron current density is considered to be simply a fraction of the incident electron current density, the same integration applies to both. The calculation for positive ion collection is the same as for electron collection with approprite sign changes to account for the positive charge, and using the ion mass and temperature. In equations (B9) to (B11), the sign on the leading charge has been suppressed. Appropriate signs will be supplied in section B.5 below.

The integration to be performed is

$$j_i = \frac{a^2}{R^2} N_i e \left(\frac{eV_i}{2\pi M_i}\right)^{1/2} \frac{2}{(eV_i)^2} \int_{\varepsilon_o}^{\infty} \int_0^{\theta_o} \sin\theta_a \cos\theta_a \varepsilon_a \exp\left(-\frac{\varepsilon_a}{eV_i}\right) d\theta_a d\varepsilon_a \tag{B12}$$

Cauffman[10] evaluates this integral and finds, in agreement with Langmuir[12].

$$j_i = j_{io} \exp\left(\frac{V_S}{V_i}\right) \qquad V_S \leq 0 \text{ (Repulsive)}$$

$$j_i = j_{io}\left(1 + \frac{V_S}{V_i}\right) \qquad V_S > 0 \text{ (Attractive)} \tag{B13}$$

where

$$j_{io} = N_i e \left(\frac{eV_i}{2\pi M_i}\right)^{1/2}$$

Since the interest here is in modelling charging in substorms with no photoemission, we expect V_S negative. Thus, electrons are repelled and ions attracted. So we have for electrons

$$j_e = j_{eo} \exp\left(\frac{V_S}{V_e}\right) \tag{B14}$$

for ions

$$j_p = j_{po}\left(1 - \frac{V_S}{V_p}\right) \tag{B15}$$

where the minus sign reflects the fact that ions are attracted by negative V_S. For backscattered electrons,

$$j_{BS} = \zeta j_e = \zeta j_{eo} \exp\left(\frac{V_S}{V_e}\right) \tag{B16}$$

where ζ is the backscatter coefficient.

B.3 SECONDARY ELECTRONS DUE TO ELECTRON IMPACT

Secondary yield as a function of electron impact energy has been given by Sternglass[8] as

$$\delta(\varepsilon_R) = 7.4\ \delta_m \frac{\varepsilon_R}{eV_m} \exp\left[-2\left(\frac{\varepsilon_R}{eV_m}\right)^{1/2}\right] \tag{A4}$$

where δ_m is the maximum yield and eV_m the energy at which the maximum yield is obtained. To determine secondary electron current density, we must multiply the left hand side of equation (B11) by $\delta(\varepsilon_R)$ and integrate. Thus, we need

$$j_s = \frac{a^2}{R^2} j_{eo} \frac{2}{(eV_e)^2} \frac{7.4\ \delta_m}{eV_m} \int_{\varepsilon}^{\infty} \int_0^{\theta_o} \varepsilon_a(\varepsilon_a + eV_S)\exp\left[-\frac{\varepsilon_a}{eV_e}\right.$$

$$\left. - 2\left(\frac{\varepsilon_a + eV_S}{eV_m}\right)^{1/2}\right] \sin\theta_a \cos\theta_a d\theta_a d\varepsilon_a \tag{B17}$$

which is Cauffman's[10] equation for secondary electrons, except that he uses a $\sec\theta_r$ dependence of δ on θ_r which is not used here. The θ_a integral is the same as before and yields

$$j_s = j_{eo} \frac{7.4\ \delta_m}{(eV_e)^2 eV_m} \int_{\varepsilon_o}^{\infty} (\varepsilon_a + eV_S)^2 \exp\left[-\frac{\varepsilon_a}{eV_e} - 2\left(\frac{\varepsilon_a + eV_S}{eV_m}\right)^{1/2}\right] d\varepsilon_a \tag{B18}$$

Now, sequentially setting $x^2 = \varepsilon_a + eV_S$ and $\eta = (eV_e)^{-1/2}x + (V_e/V_m)^{1/2}$ and substituting, we find

$$j_s = 2\ j_{eo}\ 7.4\ \delta_m \frac{V_e}{V_m} \exp\left(\frac{V_S}{V_e} + \frac{V_e}{V_m}\right) \int_{\eta_o}^{\infty} \left[\eta - \left(\frac{V_e}{V_m}\right)^{1/2}\right]^5 \exp(-\eta^2)\, d\eta \tag{B19}$$

where

$$\eta_o = \begin{cases} \left(\frac{V_S}{V_e}\right)^{1/2} + \left(\frac{V_e}{V_m}\right)^{1/2} & \text{for} \quad V_S > 0 \\ \left(\frac{V_e}{V_m}\right)^{1/2} & \text{for} \quad V_S \leq 0 \end{cases}$$

Since we are considering substorm cases only here, the condition $V_S \leq 0$ is of interest. For this case the integral in (B19) is just

$$J = \int_{(V_e/V_m)^{1/2}}^{\infty} \left[\eta - \left(\frac{V_e}{V_m}\right)^{1/2}\right]^5 \exp(-\eta^2)\, d\eta \tag{B20}$$

Recalling the expression for repeated integrals of the error function complement[14]

$$i^n\mathrm{erfc}(z) = \frac{2}{\sqrt{\pi}} \int_z^\infty \frac{(t - z)^n}{n!} \exp(-t^2)dt \tag{B21}$$

where, by definition,

$$i^n\mathrm{erfc}(z) = \int_z^\infty L^{n-1}\mathrm{erfc}(t)dt$$

and

$$i^0\mathrm{erfc}(z) = \frac{2}{\sqrt{\pi}} \int_z^\infty \exp(-t^2)dt = \mathrm{erfc}(z)$$

and identifying t, z, and n with the appropriate variables in (B20), we have

$$\Omega = \frac{\sqrt{\pi}}{2}\, 5!\, i^5\mathrm{erfc}\left(\sqrt{\frac{V_e}{V_m}}\right) \tag{B22}$$

So, from (B19) and (B22) we have

$$j_s = \sqrt{\pi}\, j_{eo} 7.4\, \delta_m \frac{V_e}{V_m}\, 5! \left[i^5\mathrm{erfc}\left(\sqrt{\frac{V_e}{V_m}}\right)\right] \exp\left(\frac{V_S}{V_e} + \frac{V_e}{V_m}\right) \tag{B23}$$

and we note that the dependence of j_s on V_S is the same as that of j_e and j_{BS}.

B.4 LEAKAGE CURRENT DENSITY

Leakage current density is defined in the same manner for the space model as it was for the test facility model (see section A.5 above).

Thus, we have

$$j_\ell = \frac{V_S}{\rho \ell} \tag{B24}$$

where ρ is bulk resistivity and ℓ is the thickness of the insulating film.

B.5 THE 1-D SPACE MODEL

Now, the net current density to the sample surface is

$$j_c = -j_e + j_\rho + j_s + j_{BS} - j_\ell \tag{B25}$$

where the signs on the current densities are given explicity here, and we recall that V_S in this model is algebraic (i.e., can be positive or negative), although the derivations have assumed it negative.

The net current density plays the role of a charging current to the surface, so that

$$j_c = C \frac{dV_S}{dt} = -j_e + j_\rho + j_s + j_{BS} - j_\ell \tag{B26}$$

where C is capacity expressed in farads per square centimeter and where we assume we are charging a capacitor. Equation (B26) is solved in the same way as equation (A13) on a computer to determine V_S versus time for charging.

CURRENT DENSITIES TO SAMPLE

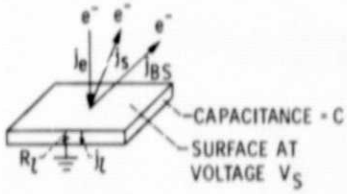

ASSUMPTIONS

MONOENERGETIC DIRECTED BEAM
NORMAL INCIDENCE ON PLANAR SAMPLES

CHARGING MODEL

$$j_e(j_s) - j_s(V_s) - j_{BS}(V_s) - j_L(V_s) + j_C(V_s, t) = j_m$$

$$I_m = Aj_m = \text{CURRENT}$$

FUNCTIONAL FORMS
DARK CONDITION → NO PHOTOEMISSION

SYMBOL & FORMULA	CURRENT DENSITY DUE TO
$j_e = j_0\left(1 - \frac{V_S}{V_B}\right)^{1/2}$	ELECTRON BEAM
$j_s = j_0\, 7.4\, \delta_m \frac{V_B}{V_m}\left(1 - \frac{V_S}{V_B}\right)^{3/2} \exp\left(-2\sqrt{\frac{V_B - V_S}{V_m}}\right)$	SECONDARY ELECTRONS
$j_{BS} = \zeta j_0\left(1 - \frac{V_S}{V_B}\right)^{1/2}$	BACKSCATTERED ELECTRONS
$j_L = \frac{V_S}{R_L A} = \frac{V_S}{\rho l} = \frac{V_S}{\rho \cdot l}$	LEAKAGE THROUGH INSULATOR
$j_C = C\frac{dV_S}{dt}$	SURFACE CHARGING

CS-78306

Figure 1. - 1-D model ground test environment.

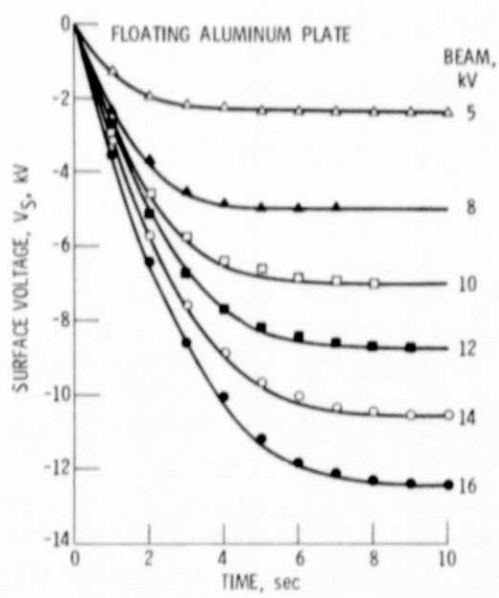

CS-78297

Figure 2. - Comparison with experimental data.

E-8970-2

REPRODUCIBILITY OF THE ORIGINAL PAGE IS POOR

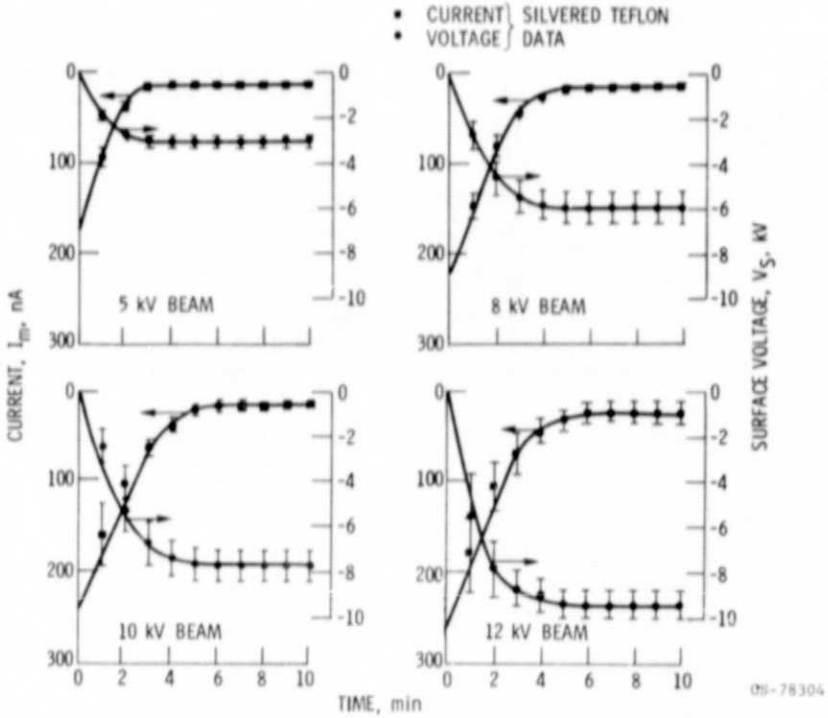

Figure 3. - Comparison with experimental data. 5 mil silvered Teflon samples; 300 cm^2 area.

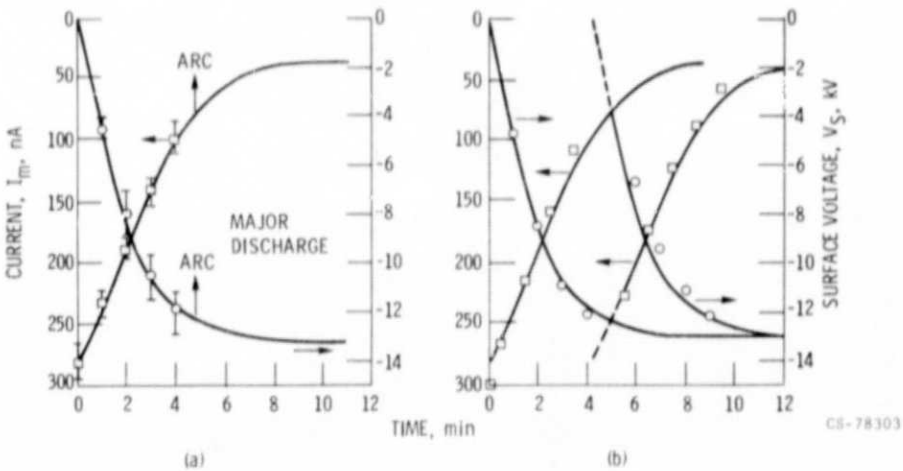

Figure 4. - Comparison with experimental data. Discharge transients; silvered Teflon samples; 16 kV beam.

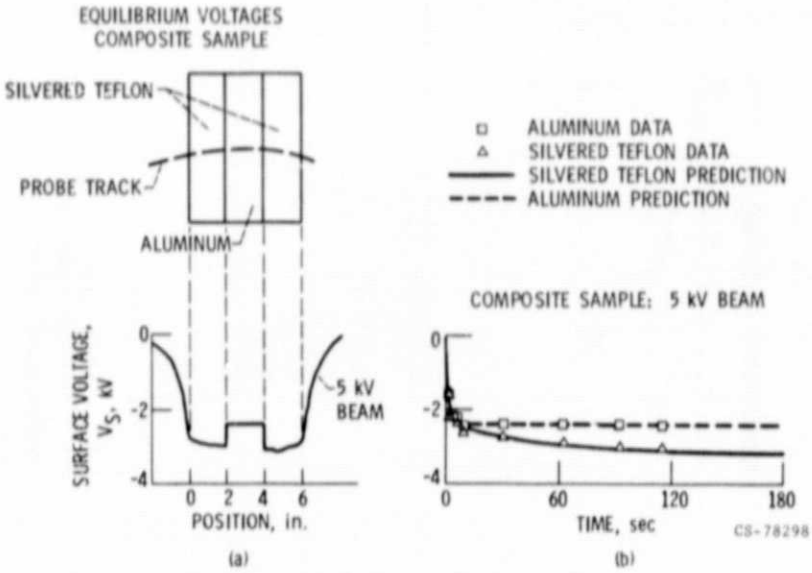

Figure 5. - Silvered Teflon/aluminum composite sample floating.

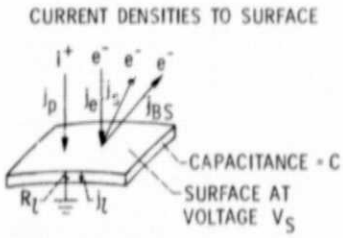

ASSUMPTIONS

GEOMAGNETIC SUBSTORM
ISOTROPIC MAXWELLIAN DISTRIBUTIONS
SPHERICAL COLLECTION GEOMETRY

CHARING MODEL

$$j_e(V_S) + j_p(V_S) + j_s(V_S) + j_{BS}(V_S) = j_l(V_S) + j_C(V_S, t)$$

FUNCTIONAL FORMS
DARK CONDITION → NO PHOTOEMISSION

SYMBOL & FORMULA	CURRENT DENSITY DUE TO
$j_e = j_{eo} \exp\left(\frac{V_S}{V_e}\right)$	PLASMA ELECTRONS
$j_p = j_{pO}\left(1 - \frac{V_S}{V_p}\right)$	PLASMA IONS
$j_s = j_{eo}\sqrt{\pi}\, 7.4\, \delta_m \frac{V_e}{V_m} 5! \left[i^5 \mathrm{erfc}\left(\sqrt{\frac{V_e}{V_m}}\right)\right] \exp\left(\frac{V_e}{V_m} + \frac{V_S}{V_e}\right)$	SECONDARY ELECTRONS
$j_{BS} = \zeta j_{eo} \exp\left(\frac{V_S}{V_e}\right)$	BACKSCATTERED ELECTRONS
$j_l = \frac{V_S}{R_l} = \frac{V_S}{\rho l}$	LEAKAGE THROUGH INSULATOR
$j_C = C \frac{dV_S}{dt}$	SURFACE CHARGING CS-78305

Figure 6. - 1-D model space substorm environment.

E-6470-2

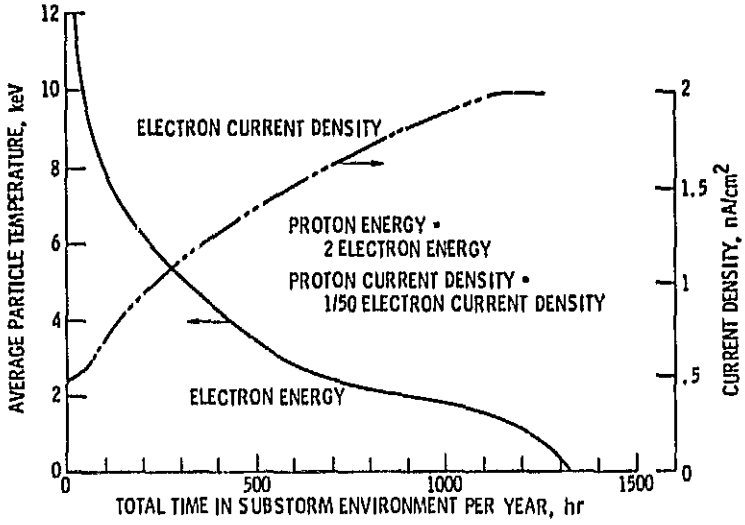

Figure 7. - Provisional specification for satellite time in a geomagnetic substorm environment (ref. 11).

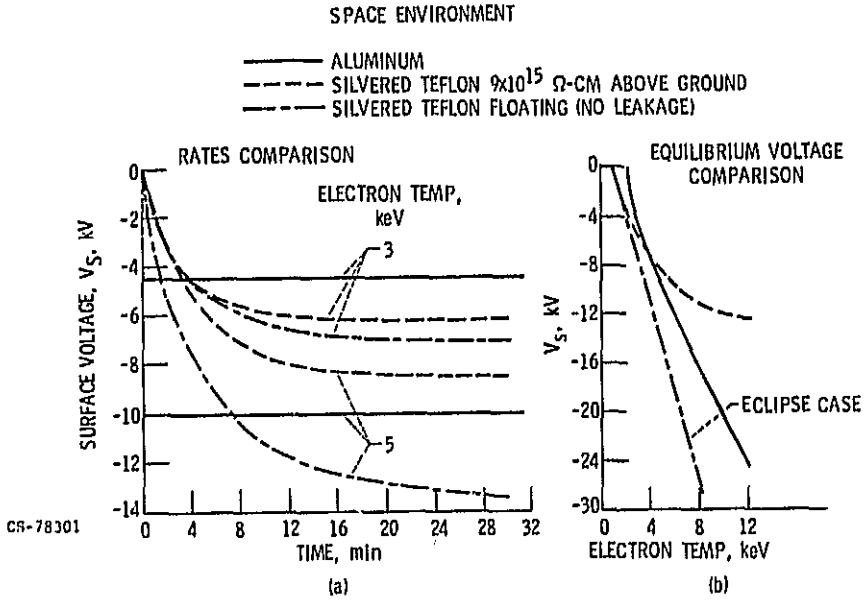

Figure 8. - Predictions of charging silvered Teflon and aluminum samples.

REPRODUCIBILITY OF THE ORIGINAL PAGE IS POOR

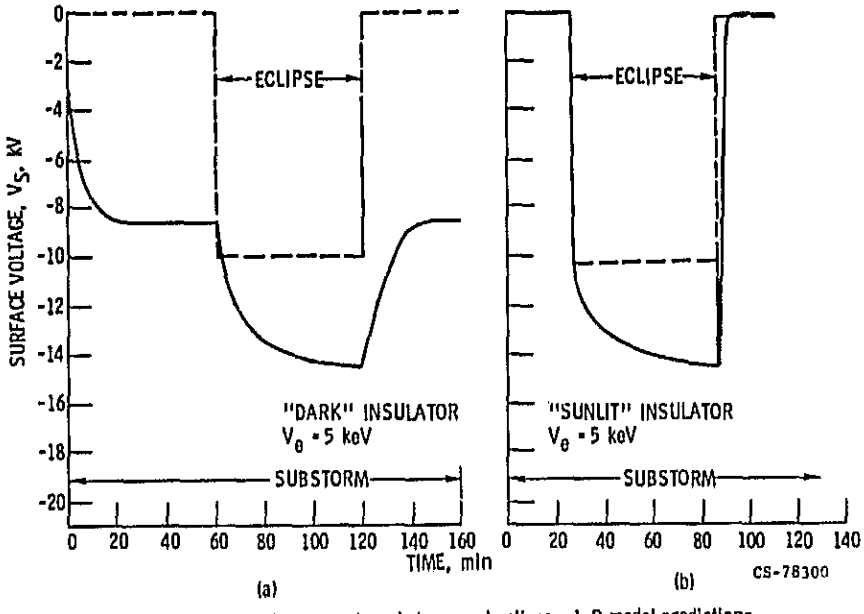

Figure 9. - Response to substorm and eclipse. 1-D model predictions.

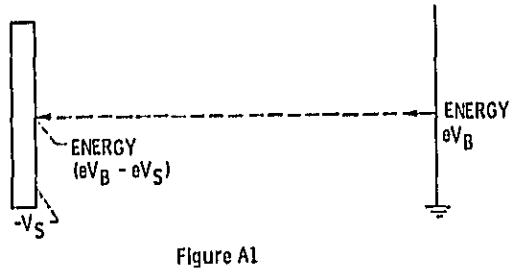

Figure A1

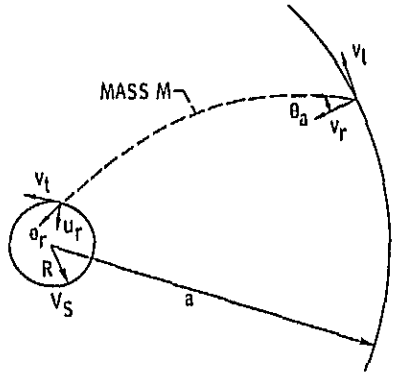

Figure B1

E-8970-2